Formation of CdSe nanoclusters in MgO by ion beam synthesis

van Huis, MA; van Veen, A; Schut, H; Eijt, SWH; Kooi, BJ; De Hosson, JTM

Published in:
Nuclear Instruments & Methods in Physics Research Section B-Beam Interactions with Materials and Atoms

DOI:
10.1016/j.nimb.2003.11.032

Publication date:
2004

Available online at www.sciencedirect.com
SCIENCE DIRECT®
Nuclear Instruments and Methods in Physics Research B 216 (2004) 121–126
NIM B
Beam Interactions with Materials & Atoms
www.elsevier.com/locate/nimb

Formation of CdSe nanoclusters in MgO by ion beam synthesis

M.A. van Huis [a,*], A. van Veen [a], H. Schut [a], S.W.H. Eijt [a], B.J. Kooi [b], J.Th.M. De Hosson [b]

[a] *Interfaculty Reactor Institute, Delft University of Technology, Mekelweg 15, 2629 JB Delft, The Netherlands*
[b] *Materials Science Center, University of Groningen, Nijenborgh 4, 9749 AG Groningen, The Netherlands*

Abstract

Embedded CdSe nanoclusters were created in MgO by ion implantation of 1×10^{16} Cd and 1×10^{16} Se ions cm $^{-2}$ at an energy of 280 and 210 keV, respectively, and subsequent thermal annealing at 1300 K. Transmission electron microscopy analysis shows that the smallest nanoclusters with sizes below 5 nm adopt a rock salt crystal structure and that the orientation relationship with the rock salt MgO is cube-on-cube. The larger nanoclusters have a different crystal structure that is sphalerite or wurtzite CdSe. The defect evolution during the annealing procedure is investigated by means of optical absorption spectroscopy and Doppler broadening positron beam analysis.

PACS: 61.46.+w; 61.72.Ji; 68.55.Ln; 78.70.B
Keywords: Ion implantation; Nanoclusters; Structural properties; Defects

1. Introduction

The optical, electrical and structural properties of nanoclusters change as a function of size, offering unique opportunities to tailor material properties for future use in applications. The electronic properties of semiconductor nanoclusters change already at sizes below 10 nm, which is larger than for the case of metals where the electronic properties show major changes only below a few nm. CdSe nanoclusters are one of the most interesting nanocluster materials. The electronic band gap changes as a function of cluster size, varying from 1.8 eV for bulk CdSe to 2.5 eV for CdSe nanoclusters with a size of 2 nm [1,2]. The crystal structure also varies as a function of cluster size [3]. One feature of nanoclusters is the large fraction of surface atoms. The first few atomic layers at the outside of the nanocluster will have other properties than the interior of the nanocluster (due to surface reconstruction, presence of defects, bending of electric bands, other charge carriers). This is not so desirable from the point of view of applications. One way to prevent surface effects, is to passivate the nanocluster surface by embedding the nanoclusters in hosts with a large band gap and similar structural properties. Ion implantation into ceramic oxides is a very practical method to create embedded, electronically passivated

* Corresponding author. Tel.: +31-15-2781612; fax: +31-15-2786422.
E-mail address: vanhuis@iri.tudelft.nl (M.A. van Huis).

0168-583X/$ - see front matter
doi:10.1016/j.nimb.2003.11.032

semiconductor nanoclusters [4,5]. MgO has a high melting temperature (>3000 K) and a large band gap of 7.8 eV. Furthermore, it is optically transparent so that the optical properties of the nanoclusters can still be investigated. In this work, CdSe nanoclusters were created in MgO by sequential Cd and Se ion implantation and subsequent thermal annealing. The defect evolution during the annealing treatment is monitored with three complementary techniques: optical absorption spectroscopy, positron annihilation spectroscopy and transmission electron microscopy.

2. Experimental

In order to create nanoclusters, monocrystalline MgO(1 0 0) samples were sequentially implanted with 1×10^{16} Cd and 1×10^{16} Se ions cm^{-2} at an energy of 280 and 210 keV, respectively. After ion implantation, isochronal annealing was performed in ambient air at temperatures up to 1500 K in steps of 200 K, during periods of 0.5 h. After ion implantation and after each annealing step, the defect evolution in the sample was monitored using optical absorption spectroscopy and Doppler broadening positron beam analysis (PBA) [6]. PBA is a very sensitive positron annihilation technique for detection of ion implantation damage. The so-called S (shape) parameter is deduced from the Doppler broadening of the 511 keV annihilation peak and indicates the relative contribution of valence electrons to the annihilation spectrum. Positrons that are implanted in a material preferably trap in vacancies and vacancy clusters, where they mainly annihilate with valence electrons. This leads to an increase in the S parameter in comparison to defect-free material, and therefore the S parameter is a good indicator of open volume defects. For the PBA measurements, a mono-energetic positron beam with a variable energy of 0–30 keV was used. One sample was examined by means of cross-sectional transmission electron microscopy (XTEM) after the 1300 K annealing step. The specimen preparation is discussed elsewhere [7]; the microscope used was a JEOL 4000 EX/II operating at 400 kV (point-to-point resolution 0.17 nm).

3. Results and discussion

3.1. SRIM simulations

The ion implantation energies were chosen in such a way that the Cd and Se ion implantation profiles overlap as much as possible. Fig. 1 shows the SRIM calculations [8] for 280 keV Cd and 210 keV Se. Here displacement energies of 55 eV were used for both the Mg and the O atoms [9]. As is clear from the figure, the straggling of the Cd profile is somewhat larger than that of the Se profile. However, during the nanocluster formation process, the atoms are somewhat mobile and this is expected to reduce a possible deviation from stoichiometry. Cd and Se have melting points (594 and 490 K, respectively) that are much lower than that of CdSe (1350 K [10]). Cd and Se nanoclusters will therefore be much less stable during thermal annealing and will easily dissociate to form CdSe nanoclusters. At the peak of the CdSe distribution, the concentration is 3.2 mol.% (CdSe per MgO).

3.2. Optical absorption spectroscopy

Fig. 2 shows the optical absorption spectra after ion implantation and after various annealing steps. After ion implantation, V-centers (Mg monovacancies) are present at a photon energy of 2.2 eV,

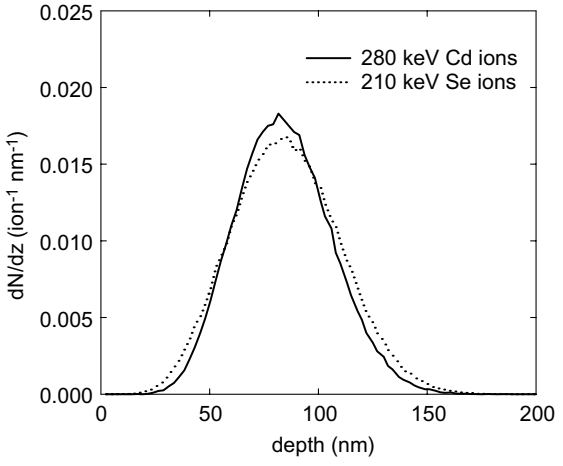

Fig. 1. Predicted depth distribution of 280 keV Cd ions and 210 keV Se ions in MgO, calculated with the SRIM code [8].

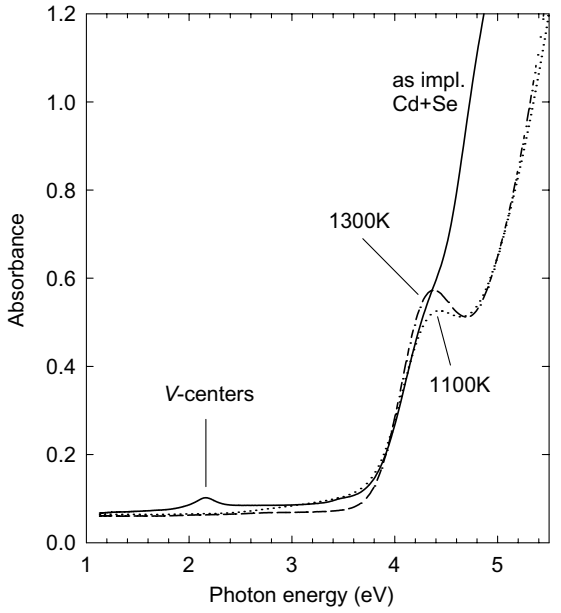

Fig. 2. Optical absorption spectra of MgO as-implanted with Cd and Se and after various annealing temperatures.

as well as F-centers (O monovacancies) at an energy of 4.9–5.0 eV. After annealing at 700 K, an absorption peak appears at 4.4 eV corresponding to Fe^{3+} impurity centers [11]. During the annealing procedure, the V-centers dissociate and the intensity of the F-centers reduces. Unfortunately, no evidence of CdSe nanoclusters can be found in the optical absorption spectra. These could be expected at an (band gap) energy in the range of 1.8–2.5 eV. It is not likely that the absorption peak at 2.2 eV in Fig. 2 corresponds to CdSe nanoclusters (instead of V-centers), because this peak disappears already after annealing at a temperature of 500 K. The broad size distribution of the CdSe nanoclusters that have been created by means of ion implantation (see the discussion of the TEM results below) will give a smeared absorption band originating from a multitude of absorption peaks rather than the presence of distinct absorption peaks. The position of the peak is dependent on the size (and therefore the band gap) of the nanocluster. For example, nanoclusters with a size of 2 nm give an absorption peak at ~2.5 eV while nanoclusters with a size of 4 nm give an absorption peak at ~2.1 eV [2]. Nevertheless, despite the size dispersion, it could still be possible to detect optical absorption by CdSe nanoclusters. In a previous work, CdSe nanoclusters were created by means of ion beam synthesis in sapphire Al_2O_3 [4] where an absorption edge was found at a wavelength of ~700 nm, corresponding to a band gap of ~1.8 eV. In the present work, the ion implantation doses are lower, indicating that the overall intensity generated by the nanoclusters is too low to be resolved.

3.3. Positron beam analysis

Fig. 3 shows the S parameter (indicator of open volume defects) as a function of positron implantation energy. The average positron implantation depth is indicated at the top of the figure. Here it should be realised that the depth resolution is limited due to the broadness of the positron implantation profile and positron diffusion processes (the resolution is approximately 20% of the implantation energy). In order to facilitate the discussion, a four-layer model is indicated in

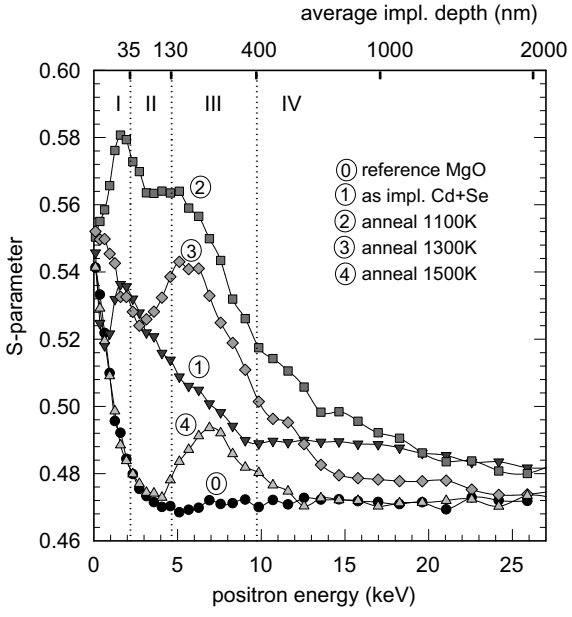

Fig. 3. S parameter as a function of positron implantation energy for the MgO sample as-implanted with Cd and Se and after annealing at various temperatures. The average positron implantation depth is indicated on top of the figure.

the figure. Layer I contains mainly displacement damage, layer II is the ion implantation range, layer III is a 'tail' of implantation defects mainly caused by channelling effects, and layer IV is the MgO bulk. The boundaries of layer II correspond reasonably well with the ion range as predicted by SRIM in Fig. 1. Directly after ion implantation, the *S* parameter in layer I–III increases due to the creation of vacancies and vacancy clusters. During the subsequent annealing steps, the *S* parameter increases further because of growth of vacancy clusters until a maximum in the *S* parameter is reached after annealing at 1100 K. At higher temperatures, the *S* parameter decreases in layers I-III because of shrinkage and dissociation of vacancy clusters. Considering the *S* parameter curve after annealing at 1300 K, it is clear that the *S* parameter in layer II (ion range) has become lower than in layers I and III (containing mainly implantation damage). Of course, layer II also contains implantation damage, but here the vacancy-type defects have recombined with the implanted Cd and Se ions so that there are less open volume defects for the positrons to become trapped in, and this results in a low *S* parameter in layer II (in comparison to the adjacent layers) after annealing at 1300 K. After annealing at 1500 K, the *S* parameter in layers I-III reduces even further.

3.4. XTEM

TEM analysis was performed on a cross-section of a sample after the 1300 K annealing step. CdSe nanoclusters with size-dependent structural properties were found, with sizes ranging from a few to 20 nm. There are three different crystal structures of CdSe: halite (cubic, rock salt), sphalerite (cubic, zinc-blende) and wurtzite (hexagonal) [2,3]. The lattice parameters of the three crystal structures are given in Table 1. The lattice parameter for rock salt CdSe is deduced from the work by Jacobs et al. [3]. Although the value of the lattice parameter is not mentioned explicitly in this work, it can be deduced from the X-ray diffraction data. The (2 0 0) peak of rock salt CdSe has a centroid at $Q = 2\pi/d_{200} = 2.24$ Å^{-1} so that $d_{\mathrm{CdSe}} = 5.61$ Å. This value does not refer to bulk CdSe, but to CdSe nanoclusters with a size of 11 ± 1 nm and at a pressure of 9 GPa.

In the high-resolution image of Fig. 4, three small CdSe nanoclusters can be observed. For all

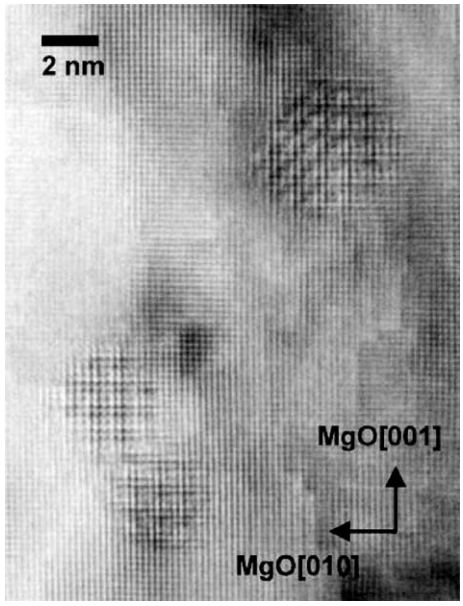

Fig. 4. High-resolution TEM image of small (<5 nm) CdSe nanoclusters with a rock salt crystal structure, showing translational moiré in both the MgO[0 0 1] and MgO[0 1 0] directions.

Table 1
Crystal structure(s) and lattice parameters of MgO and CdSe

Material	Structure	Type		Lattice parameters (Å)	$V_{\mathrm{mol.}}$ (Å^3)	Ref.
MgO	Rock salt	Halite	Cubic	*a*: 4.213	18.7	[12]
CdSe	Rock salt[a]	Halite	Cubic	*a*: 5.61[a]	44.1	[3]
	Zinc blende	Sphalerite	Cubic	*a*: 6.077	55.4	[12]
	Zincite	Wurtzite	Hexagonal	*a*: 4.298	56.1	[12]
				c: 7.002		

[a] For CdSe nanoclusters at a pressure of 9 GPa.

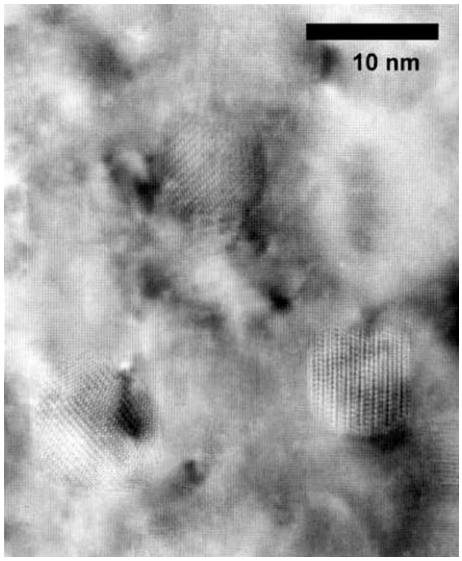

Fig. 5. High-resolution TEM image of three CdSe nanoclusters in the size range of 5–10 nm. The crystal structure of the CdSe is yet to be determined.

the nanoclusters with a size less than 5 nm, it was observed that translational moiré fringes run in both the MgO[0 1 0] and the MgO[0 0 1] directions. This shows that the CdSe crystal structure is cubic. The lattice parameter can be deduced from the spacing of the moiré fringes, using the following relationship:

$$\frac{1}{d_{\text{fringes}}} = \left| \frac{1}{d_{\text{MgO}}} - \frac{1}{d_{\text{CdSe}}} \right|. \quad (1)$$

MgO has a lattice parameter of 4.213 Å so that $d_{\text{MgO}(0\,0\,2)} = 2.107$ Å. From Fig. 4, it is clear that there are exactly 4 MgO fringes per moiré fringe. This means for CdSe that $d_{\text{CdSe}} = 4/3 \cdot d_{\text{MgO}(0\,0\,2)} = 2.81$ Å. Table 1 gives a lattice parameter of rock salt CdSe of 5.61 Å so that $d_{\text{CdSe}(0\,0\,2)} = 2.81$ Å, which coincides with the value calculated from the moiré fringes. From the observations above it is also clear that the clusters are in a cube-on-cube orientation relationship with the MgO host. Rock salt CdSe is more ionic than sphalerite or wurtzite CdSe so that it fits better in the ionic MgO lattice. Moreover, the smallest nanoclusters experience the largest pressure, and rock salt CdSe is more densily packed than the other structures. The molecular volume of rock salt CdSe is at least 20% smaller than the molecular volume of the sphalerite or wurtzite phase (see Table 1). This explains why the smallest clusters have the rock salt structure as a preferred orientation despite the very large lattice mismatch with MgO of 33% (calculated as $(d_{\text{CdSe}} - d_{\text{MgO}})/d_{\text{MgO}}$).

Fig. 5 shows three CdSe nanoclusters with sizes of 5–10 nm. Here moiré fringes and high-resolution interference patterns are observed. These clusters have the sphalerite or the wurtzite crystal structure, but currently we cannot identify which of the two is present. The orientation relationship in case of sphalerite is observed as $(1\,1\,1)_{\text{s}} \parallel (0\,0\,2)_{\text{MgO}}$, $[1\,1\,\bar{2}]_{\text{s}} \parallel [1\,0\,0]_{\text{MgO}}$ and in case of wurtzite as $(0\,0\,0\,2)_{\text{w}} \parallel (0\,0\,2)_{\text{MgO}}$, $[1\,1\,\bar{2}\,0]_{\text{w}} \parallel [1\,0\,0]_{\text{MgO}}$. More extensive TEM analysis is required to determine the crystal structure of the larger CdSe nanoclusters.

4. Conclusions

CdSe nanoclusters were successfully created in MgO by means of ion beam synthesis with post-implantation thermal annealing at 1300 K. The CdSe nanoclusters have a broad size distribution of 2–20 nm. The clusters that are smaller than 5 nm have the rock salt crystal structure and are in a cube-on-cube orientation relationship with the MgO host matrix. More experimental and analytical work is needed to distinguish between the sphalerite or wurtzite crystal structure for the larger clusters. No optical absorption peaks could be found that can be attributed to CdSe, which is probably due to the broad size distribution and a too low number of nanoclusters.

References

[1] A.P. Alivisatos, Science 271 (1996) 933.
[2] A.P. Alivisatos, J. Phys. Chem. 100 (1996) 13226.
[3] K. Jacobs, J. Wickham, A.P. Alivisatos, J. Phys. Chem. B 106 (2002) 3759.
[4] C.W. White, J.D. Budai, S.P. Withrow, J.G. Zhu, E. Sonder, R.A. Zuhr, A. Meldrum, D.M. Hembree Jr., D.O. Henderson, S. Prawer, Nucl. Instr. and Meth. B 141 (1998) 228.
[5] C.W. White, A. Meldrum, J.D. Budai, S.P. Withrow, E. Sonder, R.A. Zuhr, D.M. Hembree Jr., M. Wu, D.O. Henderson, Nucl. Instr. and Meth. B 148 (1999) 991.

[6] A. van Veen, H. Schut, P.E. Mijnarends, in: P.G. Coleman (Ed.), Positron Beams and their Applications, World Scientific, Singapore, 2000, p. 191, Chapter 6.
[7] B.J. Kooi, A. van Veen, J.Th.M. De Hosson, H. Schut, A.V. Fedorov, F. Labohm, Appl. Phys. Lett. 76 (9) (2000) 1110.
[8] J.F. Ziegler, J.P. Biersack, U. Littmark, The Stopping and Range of Ions in Solids, Pergamon, New York, 1985.
[9] S.J. Zinkle, C. Kinoshita, J. Nucl. Mater. 251 (1997) 200.
[10] Handbook of Chemistry and Physics, 56th ed., CRC press, USA, 1975.
[11] W.C. Las, T.G. Stoebe, Radiat. Protect. Dosimetry 8 (1984) 45.
[12] JCPDS file 04-0829 (for MgO), file 19-0191 (for sphalerite CdSe) and file 08-0459 (for wurtzite CdSe), International Centre for Diffraction Data, 1997.